

Research Article

Effects of Synthetic Procedures and Postsynthesis Incubation pH on Size, Shape, and Antibacterial Activity of Copper (I) Oxide Nanoparticles

Vinh Tien Nguyen  and Khanh Son Trinh 

Faculty of Chemical and Food Technology, Ho Chi Minh City University of Technology and Education, 1 Vo Van Ngan Street, Linh Chieu Ward, Thu Duc District, Ho Chi Minh City, Vietnam

Correspondence should be addressed to Khanh Son Trinh; sontk@hcmute.edu.vn

Received 26 February 2020; Revised 6 April 2020; Accepted 18 April 2020; Published 8 June 2020

Academic Editor: Nenad Ignjatović

Copyright © 2020 Vinh Tien Nguyen and Khanh Son Trinh. This is an open access article distributed under the Creative Commons Attribution License, which permits unrestricted use, distribution, and reproduction in any medium, provided the original work is properly cited.

Copper (I) oxide nanoparticles (Cu_2O NP) were synthesized by reducing CuSO_4 with glucose in the presence of polyvinyl alcohol as a capping agent. We used three different synthetic procedures with a fast reaction (procedure 1*p*), a fast-then-slow reaction (procedure 2*p*), and a slow-then-fast reaction (procedure 3*p*). The reaction rates were controlled by changing the temperature and the speed of adding reagents. The synthesized Cu_2O NP were subsequently incubated for 24 h in a pH 6 solution (Cu_2O NP6) or a pH 8 solution (Cu_2O NP8) at 5°C. XRD and SEM images analysis revealed that the 1*p* procedure produced smaller NP, while the 2*p* procedure produced larger but more uniform NP. The 3*p* procedure produced the largest NP with a higher size variation. The 24-hour acidic postsynthesis incubation resulted in an etching effect, which reduced the size and size variation of Cu_2O NP6. To evaluate the antibacterial activity, *E. coli* suspensions were mixed with the obtained Cu_2O NP (32, 96, or 160 ppm) for different time intervals (1 or 24 h) and then grown on Petri dishes at 37°C for 24 h. Higher doses, smaller sizes of Cu_2O NP, and longer contact times with the bacterial suspension resulted in higher inactivation efficiencies. Cu_2O NP6 showed higher antibacterial effects at low doses, possibly due to the etching effect and the positive surface charge. Increasing the Cu_2O doses from 32 to 96 and 160 ppm noticeably increased the antibacterial effect of the Cu_2O NP8, but not significantly for Cu_2O NP6. We suggested that the Cu_2O NP6 suffered from agglomeration at high doses due to their high surface activity and low surface charges.

1. Introduction

One of the main problems with conventional antibiotics is that their extensive and prolonged use results in the resistance of various infectious bacterial strains against them [1]. Antibacterial nanomaterials have emerged with many advantages, including high effectiveness, robustness, variety, and low doses [2]. Metallic-based antibacterial nanomaterials are mostly made from transition metals such as silver, zinc, gold, and copper [3]. Silver in recent decades has proved to be a highly effective biocidal agent, but with two major drawbacks: high price and lack of a proper requisition channel resulting in high toxicity [4]. Copper-based nanomaterials can overcome these problems because they are abundant, have low-cost, and can be expelled out of the body [5]. Among copper compounds,

copper oxides have emerged as excellent nanomaterials for antibacterial applications because of their high antibacterial effectiveness and storage stability [6]. Cuprous oxide Cu_2O was found to be more effective than cupric oxide CuO in antibacterial activity [7, 8]. Cu_2O has shown biocidal effects against a wide range of microorganisms, including pathogenic bacteria [9–11], fungi [12, 13], and viruses [11].

Besides complicated methods or those requiring special equipment, such as physical [14], electrochemical [15], photochemical [16], and sonochemical [17] techniques, the wet chemical approach is simpler and easier to control and scale up the Cu_2O nanoparticles (NP) production [18]. The most common precursors for Cu_2O NP synthesis are copper (II) salts (CuSO_4 , CuCl_2 , and $\text{Cu}(\text{NO}_3)_2$ or $(\text{CH}_3\text{COO})_2\text{Cu}$), and the common reducing agents are sodium borohydride, hydrazine,

1,2-hexadecanediol, glucose, ascorbic acid, CO, or borane compounds [19]. Among these reducing agents, glucose is the cheapest, environmentally green, and highly selective in producing Cu₂O [20]. The synthesis of Cu₂O NP usually requires one or more capping agents to control their shapes and sizes and prevent their agglomeration [21].

The classic LaMer mechanism of NP formation includes nucleation and growth stages, each of which can affect the size of NP. A fast reaction induced by high temperature and quick all-at-once mixing of reagents produces a burst of small nuclei in the nucleation stage and subsequent growth of these nuclei. Such fast one-step procedures usually produce small NP with a wide size distribution [22]. The size distribution of NP products can be narrower if the reaction is conducted using the extended LaMer mechanism: quickly mixing a portion of the reagents at a high temperature to produce a high amount of small nuclei first, and then slowly adding the remaining reagents at low temperature for uniform growth of the produced nuclei [23]. If the temperature is raised after the NP are formed, Ostwald ripening happens, where larger particles continue to grow with the material dissolved from the smaller particles. As a result, in the short term, the large particles become larger and the small particles become smaller, thus widening the size distribution of the NP [24]. In this study, we tested these three concepts on the synthesis of Cu₂O NP using glucose as the reducing agent, copper sulfate as the precursor, and polyvinyl alcohol (PVA) as the capping agent.

Furthermore, the size of Cu₂O NP can also be affected by the environment pH after their synthesis. It is known that Cu₂O is stable in alkaline solutions and disproportionates in acidic solutions [25]. Therefore, incubating Cu₂O in a slightly acidic solution can etch the surface of Cu₂O, thus affecting its size, morphology, and chemical and microbiological activities.

To the best of our knowledge, although Cu₂O NP have been intensively investigated, there is still no research on using the postsynthesis disproportionation of Cu₂O as a technique to modify the surface and the antibacterial properties of Cu₂O NP. In this study, after preparing Cu₂O NP by the three aforementioned procedures, we incubated them in two buffers with pH of 6.0 and 8.0 and evaluated how these treatments affected the size distribution, the shapes, and the antibacterial efficiencies of the Cu₂O NP.

2. Materials and Methods

2.1. Materials. *Escherichia coli* VTCC-B-482 strain was purchased from the Microorganisms Bank of the Institute of Microbiology and Biotechnology, Hanoi National University. Glucose, CuSO₄·5H₂O, NaOH, PVA, and H₂SO₄ were purchased from Xilong Scientific Ltd. (China). All the chemicals were of analytical grade and used without further purification.

2.2. Procedures for Copper (I) Oxide Synthesis. In this study, we used three procedures modified from a published method to synthesize Cu₂O NP [26]. All the three procedures used the same two solutions: 50 mL of solution A (1.6 M PVA and 1 M glucose) and 50 mL of solution B (1.6 M PVA and 0.01 M CuSO₄). The solutions were always stirred continuously during the reaction.

The first procedure was conducted in one step at a high temperature. Both solutions A and B were heated and kept at 60°C for 15 min under continuous stirring. The temperature of 60°C was selected to avoid browning reactions of glucose at higher temperatures. Solution B was then quickly added to solution A. To trigger the reduction of copper (II) ions to Cu₂O by glucose, the mixture pH was adjusted to 10 by using a 1 M NaOH solution. After 30 min of reaction, the mixture was cooled to room temperature, adjusted to pH 6.0 or 8.0, and stored at 5°C in a refrigerator for one day (1p6 and 1p8 procedures, correspondingly).

The second procedure for Cu₂O synthesis was conducted in two steps. The first step was quick mixing of the reagents at high temperature and the second step was slow mixing of the reagents at low temperature. To do this, solution B was divided into two halves. The first half was heated to 60°C and quickly added to solution A already at 60°C. The pH was then adjusted to 10 by adding the 1 M NaOH solution. After 30 min of reaction, the mixture was cooled to room temperature and the second half of B was slowly and dropwise added from a burette for 30 min. During this process, the pH was continuously kept at 10 by adding the 1 M NaOH solution. The mixture was left reacting for 24 h, then adjusted to pH 6.0 or 8.0, and stored at 5°C for one day (2p6 and 2p8 procedures, correspondingly).

The third procedure for Cu₂O synthesis was conducted in one step at a low temperature with a subsequent Ostwald ripening of the NP at high temperature. Solutions A and B were mixed at once at room temperature, and the mixture was adjusted to pH 10. After 1 h of reaction, the mixture was heated to 80°C in a water bath to complete the reduction reaction and speed up the Ostwald ripening. The concentration of the remaining glucose was low and did not induce browning reactions even at 80°C. After 30 min, the pH was adjusted to 6.0 or 8.0 and then stored at 5°C for one day (3p6 and 3p8 procedures, correspondingly).

To prepare the Cu₂O NP samples for structural and antibacterial characterization, the solid in the reaction mixture was collected by centrifugation at 10,000 rpm for 20 min and washed with distilled water for 3 times. After that, the solid was dispersed in absolute ethanol under ultrasonication for 1 h. The dispersion was then vacuum-dried at 40°C for 8 h and stored for further characterization. Cu₂O NP samples incubated at pH 6 and pH 8 are designated as Cu₂O NP6 and NP8, respectively.

2.3. Morphology, Size, and Crystal Structure of Cu₂O NP. The morphology and the size of the Cu₂O particles were observed using a Field-Emission Scanning Electron Microscope (FE-SEM) S-4800 (Hitachi, Japan). The sizes of 400 particles were determined using ImageJ software (version K 1.45) on the FE-SEM images. The type of crystal structure and the average crystallite size of the Cu₂O NP were determined from XRD patterns recorded on an X-ray Diffractometer (D8 Advanced, Bruker, Germany) at 25°C. The 2-theta angles were scanned from 10° to 80°, with $\lambda = 0.15418$ nm. The average size of Cu₂O NP crystallites was calculated using the Scherrer formula [27]:

$$d = \frac{K \cdot \lambda}{B \cdot \cos \theta}, \quad (1)$$

where d is the average size of the crystallites (nm); K is the Scherrer constant ($K=0.94$) assuming spherical shape of the particles [28]; λ is the X-ray wavelength = 1.54178 Å for Cu $K\alpha$; and B is the full width at half maximum of the highest peak (rad).

2.4. Antibacterial Activity of Cu_2O NP. The antibacterial activity of the synthesized Cu_2O NP was evaluated on *E. coli* by mixing the NP with the bacterial suspensions at different Cu_2O contents and determining the viability of the bacteria by the colony counting method after incubation on Petri dishes [29]. Different amounts of the synthesized Cu_2O NP were added to 1% peptone solutions containing *E. coli* of about 100 CFU/mL to reach the desired copper (I) content (32, 96, and 160 ppm). After 1 or 24 h of shaking at 180 rpm and at room temperature, the mixture was added to a Nutrient Agar medium at 45°C. The mixture was then thoroughly shaken and then poured into Petri dishes. After incubating the Petri dishes at 37°C for 24 h, the number of colonies in each Petri dish was counted. The same procedure was carried out with the negative control experiment (0% growth inhibition), where Cu_2O was not added to the bacterial suspension. To compare the antibacterial activity of the Cu_2O NP with the Cu^{2+} ions, we carried out the same procedure above with Cu_2O replaced by the solution B (CuSO_4 and PVA) containing an equivalent copper amount.

The inactivation efficiency was calculated using the following formula:

$$H = \frac{A_1 - A_2}{A_1} \times 100, \quad (2)$$

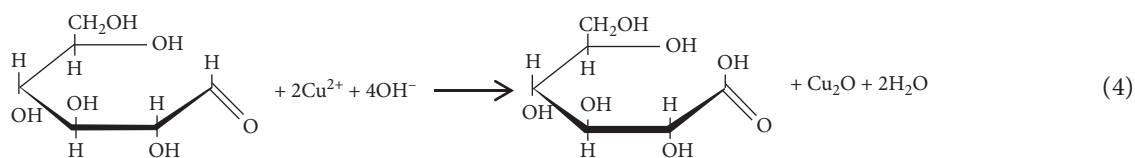
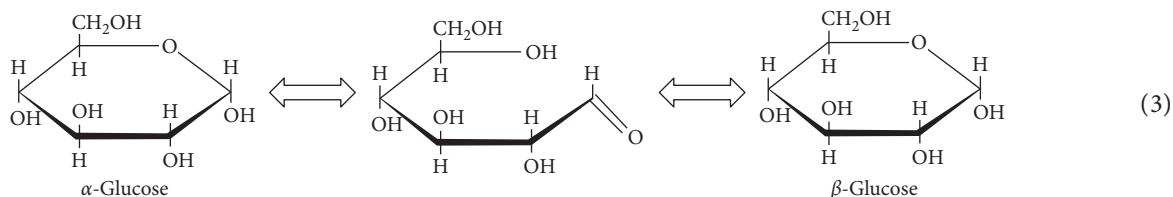
where H is the inactivation efficiency (%); A_1 is the average number of colonies on the Petri dish in the negative control experiment; and A_2 is the average number of colonies on the Petri dish after contacting the bacterial suspension with Cu_2O .

All the antibacterial experiments were replicated 3 times.

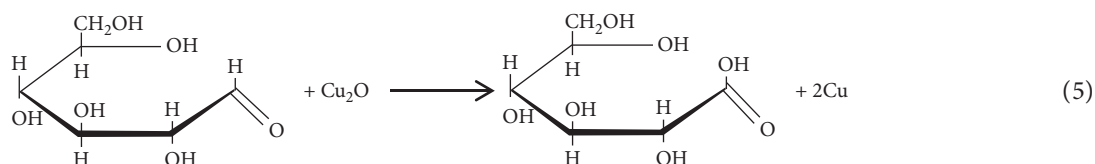
The statistical analyses of all size distributions and inactivation efficiencies of Cu_2O NP were calculated at 95% confidence level using R software package.

3. Results and Discussion

3.1. Synthesis Reactions and XRD Characterization of the Product. The reaction between a reducing sugar and copper (II) complex ions in an alkaline solution to form copper (I) oxide is the basis of the well-known Fehling and Benedict reactions. In aqueous solutions with high pH, α -glucose rings are opened and partially mutarotated into β -glucose through a chain configuration equation (3). The carbonyl group $-\text{CH}=\text{O}$ in this chain configuration of glucose can reduce copper ions to Cu_2O equation (4).



Under certain reaction conditions, the carbonyl groups can further reduce Cu_2O to metallic Cu [26, 30, 31].



Therefore, to determine the identity and the phase composition (if a mixture was formed) and to evaluate the crystallites size and shape of the obtained samples, their XRD patterns were recorded and are shown in Figure 1.

The strong and sharp peaks in the XRD patterns of all six samples show that the obtained materials were crystalline. The JCPDS Card No. 05-0667 of Cu_2O matches very well with the 2θ values of the peaks of 29.78° , 36.64° , 42.54° , 61.72° , and 73.93° , which correspond to (110), (111), (200), (220), and (311) face-centered cubic (fcc) indices, respectively [32].

The absence of other peaks in the XRD patterns indicates that the obtained samples were not contaminated with other copper compounds (Cu, CuO, or $\text{Cu}(\text{OH})_2$). This result is different from that of a study reporting the formation of solely metallic Cu (with 2θ of 43.3° , 50.4° , and 74.1°) from the reaction of copper acetate and glucose in the presence of polyvinylpyrrolidone as the protecting agent at pH 10 [26]. This difference indicates that the nature of the copper precursor and/or the protecting polymer can determine the product identity in this Fehling type of reaction.

From the average full widths at half maximum of the peaks, the average crystallite sizes of Cu_2O NP were calculated using the Scherrer equation and are shown in Table 1.

The results in Table 1 demonstrate that Cu_2O NP produced by a fast reaction (high temperature and quick mixing of reagents in procedure 1) yielded NP crystallites smaller than those produced by a slow reaction (procedures 2 and 3).

The relative intensities of (111) and (200) peaks can give some information about the shape of the Cu_2O nanocrystallites. A recent study found a noticeable relationship between the morphology of the Cu_2O NP and the relative intensities of the (200) and (111) peaks in the XRD patterns: perfect octahedral Cu_2O nanocrystals have no (200) peak, while the cubic nanocrystals have a (200) peak higher than that of (111) [33]. When the shape of Cu_2O nanocrystals evolves from octahedral through (100)-truncated octahedral to cubic, the ratio of (200):(111) peak intensities increases from 0 to nearly 2. In our study, all the samples had the (200):(111) ratios in the range 0.31–0.37, indicating the (100)-truncated octahedral morphology. Table 1 also shows that the Cu_2O NP6 had higher ratios of (200):(111) peak intensities, than the corresponding Cu_2O NP8. This result demonstrates that the acidic incubation has an etching or truncating effect on the (100) surface of the Cu_2O NP.

3.2. Morphology and Size by SEM Characterization. FE-SEM micrographs (Figure 2) of the synthesized Cu_2O materials were recorded to determine the particle sizes and morphology. In the scale of $5\ \mu\text{m}$, the Cu_2O particles prepared by the three procedures and stored at pH values of 6 and 8 had relatively uniform shapes and sizes.

The sizes of at least 400 particles for each sample were determined using the ImageJ software on the FE-SEM images. The mean, the standard deviation, and the coefficient of variation of these particle sizes are presented in Table 2.

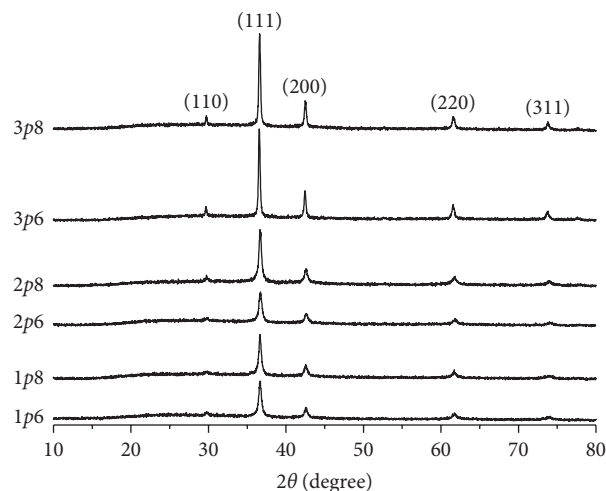


FIGURE 1: XRD patterns of Cu_2O powder samples prepared by different procedures.

TABLE 1: Average crystallite sizes of Cu_2O NP prepared by different procedures.

Procedure	1p6	1p8	2p6	2p8	3p6	3p8
Average crystallites size (nm)	12.6	12.0	12.3	14.3	26.1	23.7
Ratio of (200):(111) peak intensities	0.346	0.339	0.368	0.315	0.316	0.311

The sizes of most Cu_2O particles were in the range of 200–340 nm. In a similar study, where CuCl_2 was reduced by glucose in alkaline medium at 75°C , the sizes of Cu_2O particles were approximately $2\text{--}3\ \mu\text{m}$ [20]. The Cu_2O particle size in our study was about 10 times lower due to the use of PVA as a capping agent. This capping polymer forms a protective layer around the Cu_2O NP during the synthesis and thus prevents them from growing further [21].

Particles in sample 1p6 had significantly smaller sizes, while those in sample 3p8 had significantly larger sizes, compared to the other samples. This pattern in particle sizes is consistent with the results obtained above by XRD analysis. It should be noted that the sizes in the FE-SEM analysis are higher than those in the XRD calculations because the XRD-based sizes are of the small crystallites that agglomerated into particles observed in the FE-SEM images [34].

A comparison of the standard deviations of Cu_2O NP produced by the three procedures shows that the procedure with fast nucleation and subsequent slow growth (2p6 and 2p8) yielded particles with more uniform sizes (smaller standard deviations and coefficients of variation). This result is in accordance with LaMer theory and the practice of size-controlled NP synthesis [22]. In the first step at high temperature and quick mixing of reagents, a burst formation of small nuclei of Cu_2O occurred because of the high reaction rate between Cu^{2+} and glucose. In the second step at low temperature and slow dropwise adding of the solution B, new Cu_2O monomers were formed slowly, diffused to the surface of the above-mentioned nuclei, and deposited uniformly [22, 35]. When the Cu_2O NP

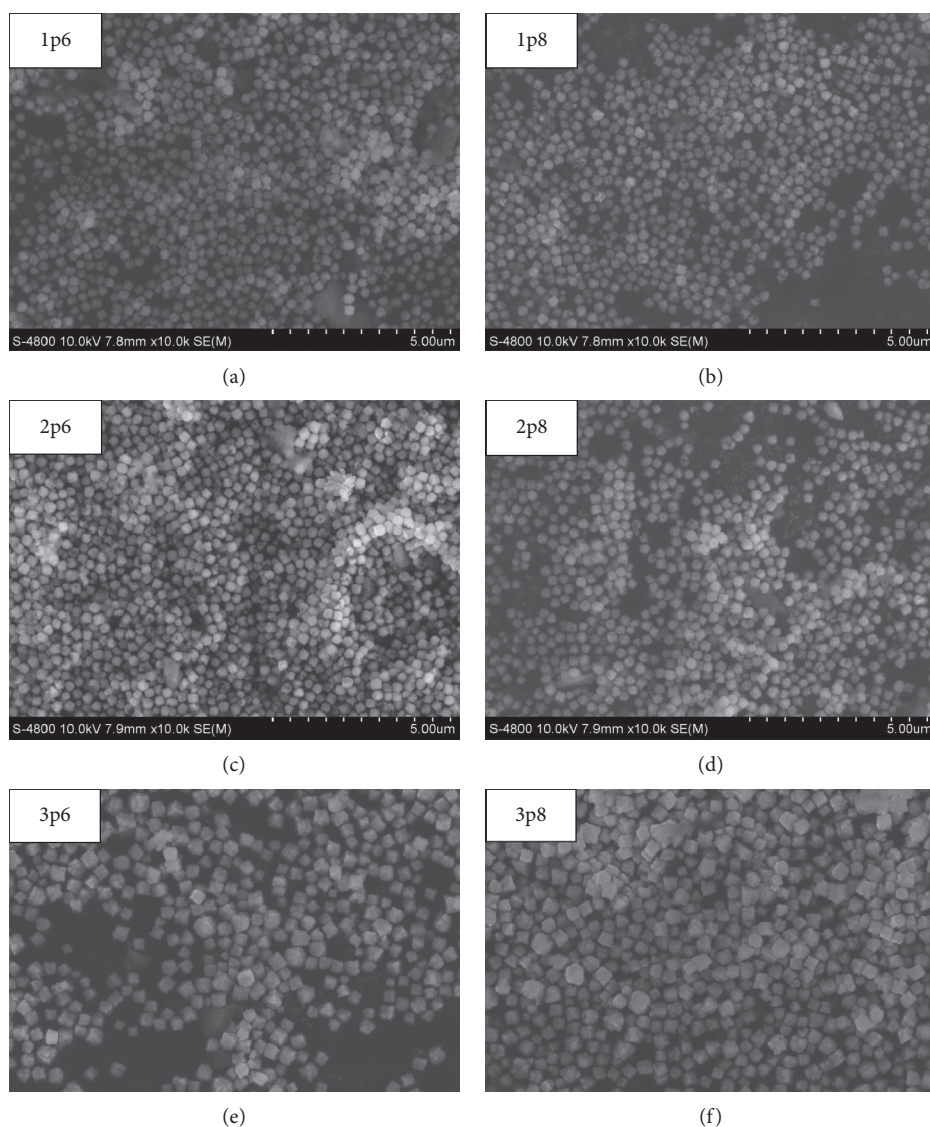


FIGURE 2: FE-SEM micrographs of Cu_2O samples at $5 \mu\text{m}$ scale (10,000x magnification): (a) 1p6, (b) 1p8, (c) 2p6, (d) 2p8, (e) 3p6, and (f) 3p8.

TABLE 2: Particle sizes (mean \pm standard deviation) of the Cu_2O samples.

Sample	1p6	1p8	2p6	2p8	3p6	3p8
Particle size (nm)	222 ± 13^a	240 ± 21^{ab}	240 ± 3^{ab}	248 ± 10^{ab}	263 ± 7^b	310 ± 33^c
Coefficient of variation (%)	5.9	8.9	1.3	4.0	2.7	10.6

Means with different superscript letters are significantly different ($p < 0.05$).

were aged at 80°C in procedure 3, Oswald ripening happened, resulting in the dissolution of smaller particles and the continued growth of larger ones [24]. As a result, the Cu_2O NP in the 3p procedures were significantly larger.

An interesting result from Table 2 is that the Cu_2O NP particles incubated in acidic solutions (pH = 6) tended to be smaller than those incubated in basic solutions (pH = 8). This is possibly because Cu_2O is stable only in an alkaline medium. In mildly acidic medium, Cu_2O disproportionates into Cu and Cu^{2+} according to reaction (6) below, resulting in an “etching” effect that reduced the Cu_2O particle size:

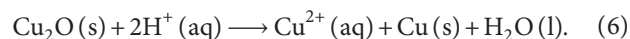


Table 2 also shows that Cu_2O NP incubated at pH 6 has smaller standard deviations in size than those incubated at pH 8. This means that acidic incubation yielded more uniform particles because the acidic etching attacked more on Cu_2O particles with a larger surface.

The etching effect of acidic incubation can be observed in the holes on the surface of Cu_2O NP (white arrows in Figure 3). This effect also existed in Cu_2O NP incubated at pH 8, but to a lesser extent. This means that Cu_2O NP also

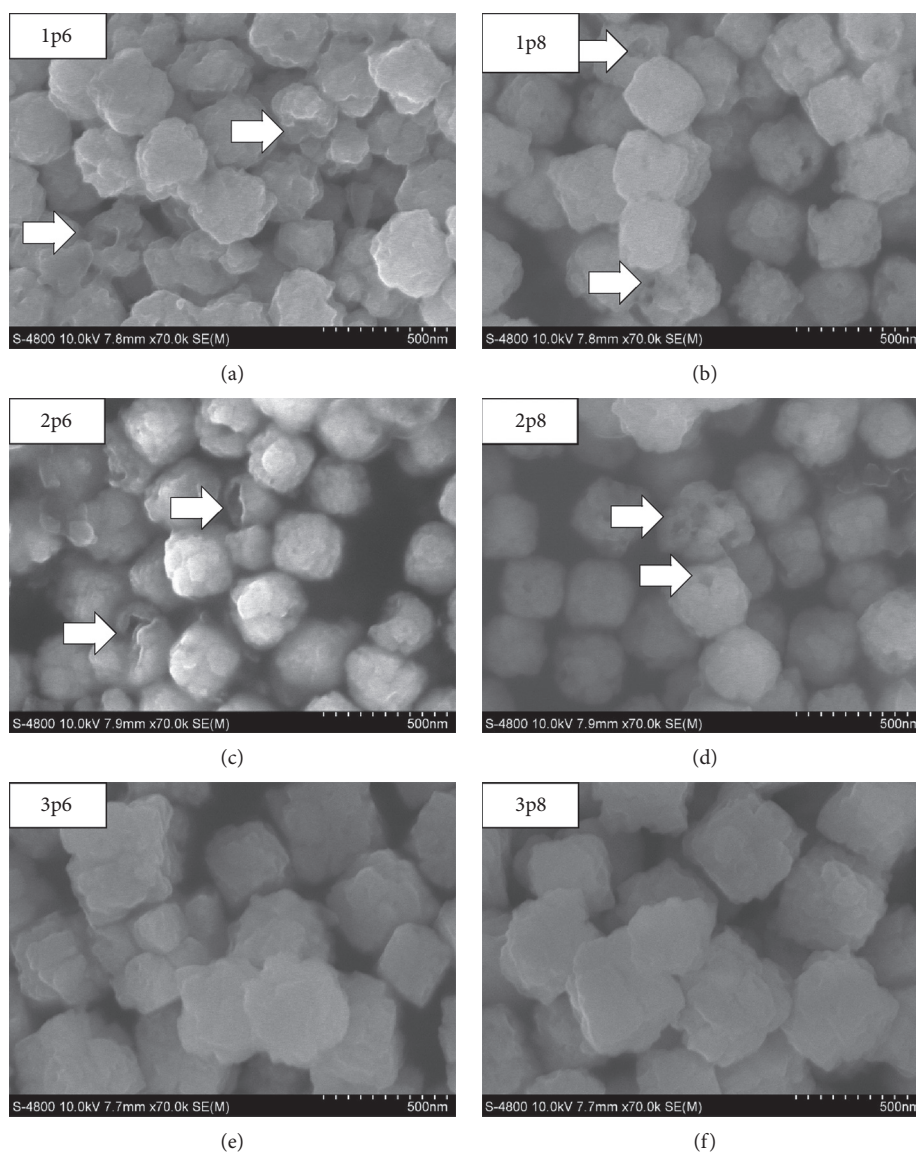


FIGURE 3: FE-SEM micrographs of Cu_2O samples at 500 nm scale (70,000x magnification): (a) 1p6, (b) 1p8, (c) 2p6, (d) 2p8, (e) 3p6, and (f) 3p8.

disproportionated in slightly basic media. It is well known that this type of defects on the surface of solids enhances their catalytic activity in chemical reactions [36, 37]. The results of acidic incubation on the sizes and size distribution imply a way of controlled surface modification to produce uniform Cu_2O NP with high surface areas and catalytic potentials.

The morphology of Cu_2O NP can be observed through FE-SEM images at 70,000x magnification (Figure 3). The shapes of Cu_2O NP synthesized by procedures 1 and 2 are close to spheres, while that of NP synthesized by procedure 3 is close to octahedral or cubes. This interesting result indicates that changing the speed of the reaction stages can alter the shape of the produced NP. A slow nucleation step followed by a fast growth step seems to yield octahedral Cu_2O crystals, while a fast nucleation step followed by a slow growing step produced spherical Cu_2O crystals [38].

3.3. Antibacterial Effects of Cu_2O NP on *E. coli*. Copper metal and its oxides are well known for their antifungal and antibacterial activities [39]. Figure 4 shows the inactivation percentage of *E. coli* after treating the bacterial suspension with the synthesized Cu_2O NP (32, 96, and 160 ppm of copper (I)) for 1 h (A and B) or 24 h (C and D). In all tested conditions, Cu_2O NP showed significantly higher inactivation efficiency compared to CuSO_4 . This is expectable, because previous studies have shown that Cu_2O is more effective than CuO [7, 8, 40] and CuO is more effective than Cu^{2+} ions in inhibiting bacterial growth [6]. Although copper ions are toxic to bacterial cells, the lipophilic cell membranes are good barriers to them. On the other hand, solid CuO or Cu_2O NP can stick to and penetrate the cell membranes and then release toxic copper ions inside the acidic lysosomes, like “Trojan-horse carriers” [41].

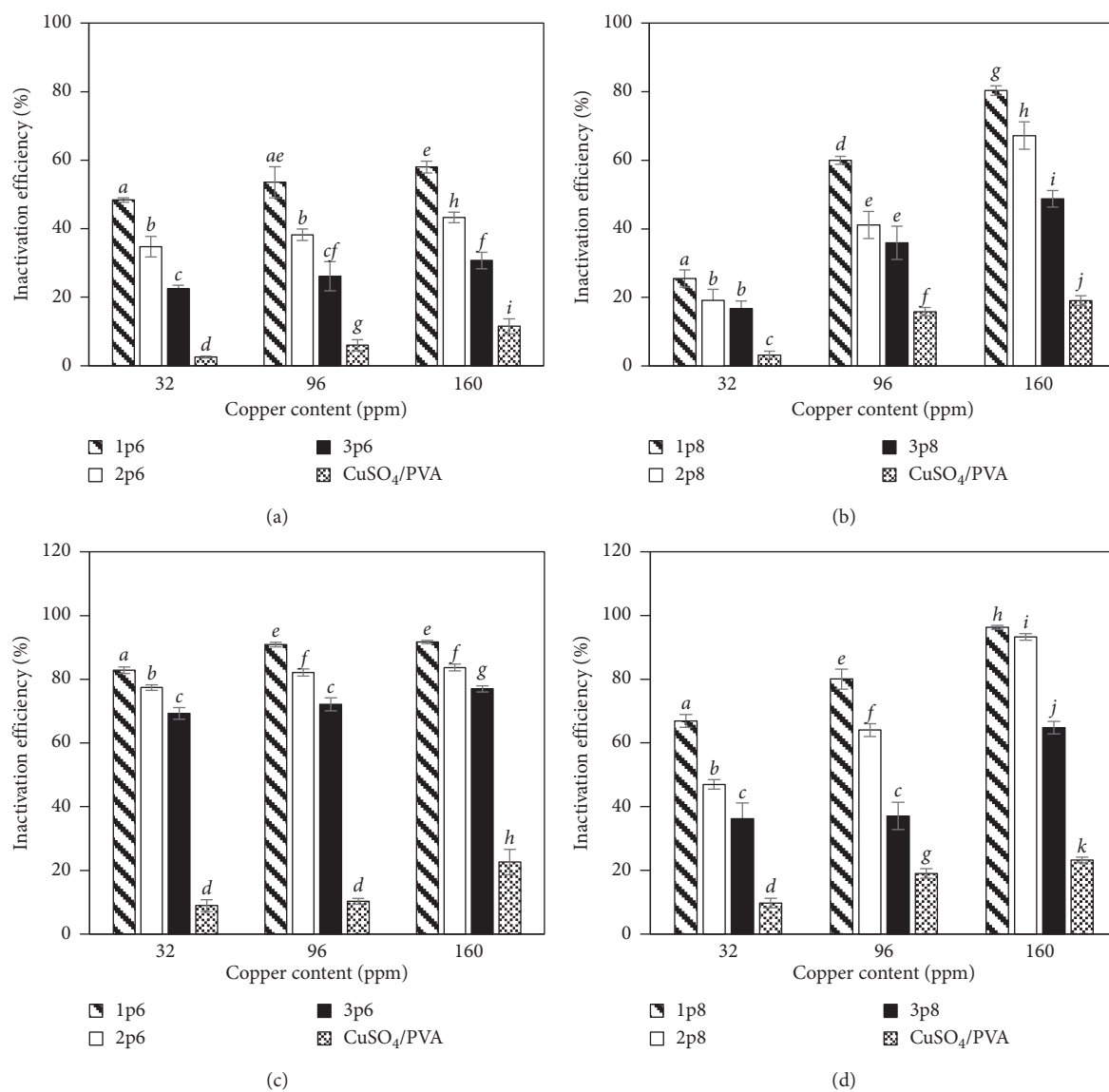


FIGURE 4: Inactivation efficiencies of Cu_2O NP incubated at pH 6 and pH 8 after 1 h and 24 h of contact with *E. coli* suspension ((a) pH6, 1 h; (b) pH8, 1 h; (c) pH6, 24 h; (d) pH8, 24 h). Different letters on the bars in the graph demonstrate significantly different inactivation efficiencies ($p < 0.05$).

A literature survey showed that the main mechanism of the antibacterial effect of Cu_2O NP is direct contact killing and the subsequent complex formation between copper (I) ions with the peptides in the cell membranes [7]. This mechanism explains the high inactivation efficiencies of Cu_2O NP with higher doses of the copper agents (Cu_2O and CuSO_4) and longer contact times (24 h compared to 1 h) with the bacterial suspension. This result is obvious because more Cu_2O NP present in the bacterial suspension and longer treatment time would increase the number of collisions and contacts between them and lead to higher antibacterial effects.

Figure 4 also shows that different procedures for Cu_2O NP synthesis resulted in significantly different inactivation efficiencies ($p < 0.05$). The decreasing order of antibacterial activity is $1p > 2p > 3p$. This order is in reverse correlation

with the mean sizes of Cu_2O NP determined in Table 2. This result is in accordance with other studies on the biocidal activities of NP, where smaller particles inactivation of microorganisms was stronger due to higher total surface areas [42–44]. In our study, the highest inactivation effect (97%) was achieved at 160 ppm of Cu_2O NP (Figure 4(d), sample 1p8) after 24 h of treatment, while in another similar study, the same effect was observed at about 13 ppm or 0.1 mM of Cu_2O NP (sizes about 40 nm) after 18 h of treatment [7]. The reason for the relatively low antibacterial efficiency in our study was the relatively high particle sizes of Cu_2O NP (240 ± 21 nm in Table 2).

For easier evaluation of the effects of the postsynthesis incubation pH on Cu_2O NP antibacterial activities, the columns in Figures 4(a)–4(d) were regrouped and represented in another way (Figure 5).

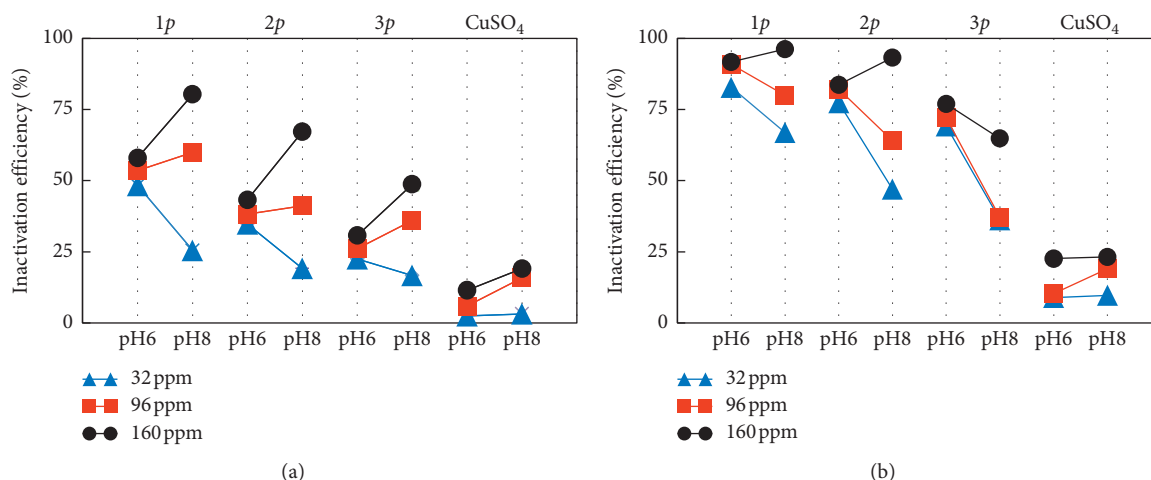


FIGURE 5: Interaction of incubation pH and copper dose on inactivation efficiency after treating *E. coli* for 1 h (a) and 24 h (b).

Figure 5 shows that there was an interaction effect of the Cu₂O NP incubation pH and their doses on *E. coli* inactivation efficiencies. After 1 h of treatment (Figure 5(a)) and at a low copper dose (32 ppm), the Cu₂O NP6 had higher inactivation efficiencies than Cu₂O NP8. However, increasing the copper dose to 96 and 160 ppm did not significantly enhance the antibacterial effect of Cu₂O NP6 but noticeably improved that of Cu₂O NP8. Eventually, the antibacterial effects of Cu₂O NP8 were higher than those of Cu₂O NP6 at 96 and 160 ppm. We suggest the following explanations for this interaction effect of copper dose and incubation pH on Cu₂O NP antibacterial effect.

The surface of Cu₂O NP6 was etched by the acidic disproportionation and became sharper with more edges and surfaces. Because the main antibacterial mechanism of Cu₂O begins with direct contact with bacterial cell walls, the edges and surfaces on the Cu₂O NP facilitate their penetration and interaction with the bacterial cell walls [7]. Another possible reason for the higher antibacterial effect of Cu₂O NP6 is that their surface was protonated and had a positive charge, while Cu₂O NP in the alkaline medium absorbed hydroxide ions and had a negative charge [45]. At the same time, the *E. coli* cell surface has a small negative charge [46] and hence interacted better with Cu₂O NP6. Therefore, Cu₂O NP6 showed higher inactivation efficiencies, compared to Cu₂O NP8 at 32 ppm.

However, increasing the dose of Cu₂O NP6 from 32 to 96 and 160 ppm did not significantly improve the antibacterial effect. This was possibly because a higher concentration of Cu₂O NP6 resulted in a higher chance of their collisions and agglomeration. We suggest that the positive surface charge of Cu₂O NP6 is smaller in magnitude, compared with the negative surface charge of Cu₂O NP8; therefore, Cu₂O NP6 are easier to agglomerate. The result of this agglomeration was a smaller amount of freely moving Cu₂O particles that can get in contact with the bacterial cells. We suggest further measurement of the zeta potential of Cu₂O NP6 and NP8 to confirm the hypothesis mentioned above.

A comparison of NP6 and NP8 in Figures 5(a) and 5(b) at the same synthetic procedure and dose shows that

NP6 samples demonstrated higher increase in inactivation efficiencies when the treatment time increased from 1 h to 24 h. For example, at the same 96 ppm dose treatments (red lines in Figure 5), the inactivation efficiencies of NP6 were lower after 1 h and higher after 24 h than those of NP8. In other words, Cu₂O “won” in the long-term antibacterial effects. For the case of 32 ppm dose, the reason mentioned above for higher efficiencies of NP6 over NP8 can be applied. For the cases of 96 and 160 ppm doses, we suggest that, during 24 h of shaking, the initial agglomerates of Cu₂O NP6 gradually disintegrated and released more bactericidal Cu₂O NP6. However, further experiments are required to test this hypothesis.

4. Conclusions

In this study, we investigated the effects of three different synthetic procedures on the size distribution of Cu₂O NP prepared by reducing CuSO₄ with glucose in an alkaline medium in the presence of PVA capping agent. The one-step procedure at high reaction rate yielded Cu₂O NP with the lowest sizes, while a fast-then-slow procedure yielded more uniform particles in size. The synthesis at a low temperature with subsequent Ostwald ripening at a high temperature produced the largest Cu₂O NP. The different procedures also yielded NP with different shapes. Moreover, postsynthesis incubation of Cu₂O NP in acidic or basic solutions also affects the size distribution as well as the antibacterial activity of these NP. Incubating Cu₂O NP in an acidic solution resulted in an etching effect on the Cu₂O NP size and size distribution. Moreover, acidic incubation of Cu₂O NP increased their antibacterial activity, possibly due to the formation of sharp edges and positive charges on the Cu₂O surface. However, increasing the doses of the acid-incubated Cu₂O NP increased the antibacterial effect not significantly, possibly due to agglomeration of the Cu₂O NP. Further investigations are required to clarify the unsolved hypotheses suggested in this study.

Data Availability

The data used to support the findings of this study are available from the corresponding author upon request.

Conflicts of Interest

The authors declare that there are no conflicts of interest regarding the publication of this paper.

Acknowledgments

The authors gratefully thank the Ho Chi Minh City University of Technology and Education for financial and facility support in completing this research. The authors thank Ms. Tran Thi Tuong Vi and Ms. Tran Thi Ngoc Han for their helpful technical assistance.

References

- [1] F. C. Tenover, "Development and spread of bacterial resistance to antimicrobial agents: an overview," *Clinical Infectious Diseases*, vol. 33, no. s3, pp. S108–S115, 2001.
- [2] D. Campoccia, L. Montanaro, and C. R. Arciola, "A review of the biomaterials technologies for infection-resistant surfaces," *Biomaterials*, vol. 34, no. 34, pp. 8533–8554, 2013.
- [3] F. Paladini, M. Pollini, A. Sannino, and L. Ambrosio, "Metal-based antibacterial substrates for biomedical applications," *Biomacromolecules*, vol. 16, no. 7, pp. 1873–1885, 2015.
- [4] A. Syafiuddin, Salmiati, M. R. Salim, A. Beng Hong Kueh, T. Hadibarata, and H. Nur, "A review of silver nanoparticles: research trends, global consumption, synthesis, properties, and future challenges," *Journal of the Chinese Chemical Society*, vol. 64, no. 7, pp. 732–756, 2017.
- [5] S. Mallick, S. Sharma, M. Banerjee, S. S. Ghosh, A. Chattopadhyay, and A. Paul, "Iodine-stabilized Cu nanoparticle chitosan composite for antibacterial applications," *ACS Applied Materials & Interfaces*, vol. 4, no. 3, pp. 1313–1323, 2012.
- [6] H. L. Karlsson, P. Cronholm, J. Gustafsson, and L. Möller, "Copper oxide nanoparticles are highly toxic: a comparison between metal oxide nanoparticles and carbon nanotubes," *Chemical Research in Toxicology*, vol. 21, no. 9, pp. 1726–1732, 2008.
- [7] S. Meghana, P. Kabra, S. Chakraborty, and N. Padmavathy, "Understanding the pathway of antibacterial activity of copper oxide nanoparticles," *RSC Advances*, vol. 5, no. 16, pp. 12293–12299, 2015.
- [8] H.-J. Park, T. T. M. Nguyen, J. Yoon, and C. Lee, "Role of reactive oxygen species in *Escherichia coli* Inactivation by cupric ion," *Environmental Science & Technology*, vol. 46, no. 20, pp. 11299–11304, 2012.
- [9] A. P. Ingle, N. Duran, and M. Rai, "Bioactivity, mechanism of action, and cytotoxicity of copper-based nanoparticles: a review," *Applied Microbiology and Biotechnology*, vol. 98, no. 3, pp. 1001–1009, 2014.
- [10] H. Pang, F. Gao, and Q. Lu, "Morphology effect on antibacterial activity of cuprous oxide," *Chemical Communications*, no. 9, pp. 1076–1078, 2009.
- [11] K. Sunada, M. Minoshima, and K. Hashimoto, "Highly efficient antiviral and antibacterial activities of solid-state cuprous compounds," *Journal of Hazardous Materials*, vol. 235–236, pp. 265–270, 2012.
- [12] B. D. Du, D. T. B. Ngoc, N. D. Thang, L. N. A. Tuan, B. D. Thach, and N. Q. Hien, "Synthesis and *in vitro* antifungal efficiency of alginate-stabilized Cu₂O-Cu nanoparticles against *Neoscytalidium dimidiatum* causing brown spot disease on dragon fruit plants (*Hyalocereus undatus*)," *Vietnam Journal of Chemistry*, vol. 57, no. 3, pp. 318–323, 2019.
- [13] K. Giannousi, G. Sarafidis, S. Mourdikoudis, A. Pantazaki, and C. Dendrinou-Samara, "Selective synthesis of Cu₂O and Cu/Cu₂O NPs: antifungal activity to yeast *Saccharomyces cerevisiae* and DNA interaction," *Inorganic Chemistry*, vol. 53, no. 18, pp. 9657–9666, 2014.
- [14] J.-K. Lung, J.-C. Huang, D.-C. Tien et al., "Preparation of gold nanoparticles by arc discharge in water," *Journal of Alloys and Compounds*, vol. 434–435, pp. 655–658, 2007.
- [15] S. Rahmah and F. Kurniawan, "Electrochemical methods for manufacturing silver nanoparticles," in *Proceedings of the 5th SEA-DR (South East Asia Development Research) International Conference 2017 (SEADRIC 2017)*, Banjarmasin, Indonesia, May 2017.
- [16] J. S. Gabriel, V. A. M. Gonzaga, A. L. Poli, and C. C. Schmitt, "Photochemical synthesis of silver nanoparticles on chitosans/montmorillonite nanocomposite films and antibacterial activity," *Carbohydrate Polymers*, vol. 171, pp. 202–210, 2017.
- [17] S. Ganguly, P. Das, M. Bose et al., "Sonochemical green reduction to prepare Ag nanoparticles decorated graphene sheets for catalytic performance and antibacterial application," *Ultrasonics Sonochemistry*, vol. 39, pp. 577–588, 2017.
- [18] A. P. Reverberi, N. T. Kuznetsov, V. P. Meshalkin, M. Salerno, and B. Fabiano, "Systematical analysis of chemical methods in metal nanoparticles synthesis," *Theoretical Foundations of Chemical Engineering*, vol. 50, no. 1, pp. 59–66, 2016.
- [19] M. B. Gawande, A. Goswami, F.-X. Felpin et al., "Cu and Cu-based nanoparticles: synthesis and applications in catalysis," *Chemical Reviews*, vol. 116, no. 6, pp. 3722–3811, 2016.
- [20] X. Han, F. Liao, Y. Zhang, Z. Yuan, H. Chen, and C. Xu, "Rapid and template-free synthesis of Cu₂O truncated octahedra using glucose as green reducing agent," *Materials Letters*, vol. 210, pp. 31–34, 2018.
- [21] C. M. Phan and H. M. Nguyen, "Role of capping agent in wet synthesis of nanoparticles," *The Journal of Physical Chemistry A*, vol. 121, no. 17, pp. 3213–3219, 2017.
- [22] V. K. LaMer and R. H. Dinegar, "Theory, production and mechanism of formation of monodispersed hydrosols," *Journal of the American Chemical Society*, vol. 72, no. 11, pp. 4847–4854, 1950.
- [23] E. C. Vreeland, J. Watt, G. B. Schober et al., "Enhanced nanoparticle size control by extending LaMer's mechanism," *Chemistry of Materials*, vol. 27, no. 17, pp. 6059–6066, 2015.
- [24] T. Sugimoto, "Preparation of monodispersed colloidal particles," *Advances in Colloid and Interface Science*, vol. 28, pp. 65–108, 1987.
- [25] L. Zhang, Q. Li, H. Xue, and H. Pang, "Fabrication of Cu₂O-based materials for lithium-ion batteries," *ChemSusChem*, vol. 11, no. 10, pp. 1581–1599, 2018.
- [26] L. S. B. Upadhyay and N. Kumar, "Green synthesis of copper nanoparticle using glucose and polyvinylpyrrolidone (PVP)," *Inorganic and Nano-Metal Chemistry*, vol. 47, no. 10, pp. 1436–1440, 2017.
- [27] P. Moeck, Y. Waseda, E. Matsubara, and K. Shinoda, "Yoshio waseda, eiichiro matsubara, kozo shinoda, X-ray diffraction crystallography," *Crystal Research and Technology*, vol. 47, no. 11, pp. 1210–1211, 2012.
- [28] C. Suryanarayana and M. Grant Norton, *X-Ray Diffraction: A Practical Approach*, Springer, Berlin, Germany, 2013.

- [29] A. Hitchins, *Bacteriological Analytical Manual*, Food and Drug Administration, Washington, DC, USA, 1998.
- [30] S. Li, Y. Chen, L. Huang, and D. Pan, "Large-scale synthesis of well-dispersed copper nanowires in an electric pressure cooker and their application in transparent and conductive networks," *Inorganic Chemistry*, vol. 53, no. 9, pp. 4440–4444, 2014.
- [31] V. Andal and G. Buvaneswari, "Effect of reducing agents in the conversion of Cu_2O nanocolloid to Cu nanocolloid," *Engineering Science and Technology, an International Journal*, vol. 20, no. 1, pp. 340–344, 2017.
- [32] A. K. Sasmal, S. Dutta, and T. Pal, "A ternary Cu_2O -Cu-CuO nanocomposite: a catalyst with intriguing activity," *Dalton Transactions*, vol. 45, no. 7, pp. 3139–3150, 2016.
- [33] S. Thoka, A.-T. Lee, and M. H. Huang, "Scalable synthesis of size-tunable small Cu_2O nanocubes and octahedra for facet-dependent optical characterization and pseudomorphic conversion to Cu nanocrystals," *ACS Sustainable Chemistry & Engineering*, vol. 7, no. 12, pp. 10467–10476, 2019.
- [34] S. Mourdikoudis, R. M. Pallares, and N. T. K. Thanh, "Characterization techniques for nanoparticles: comparison and complementarity upon studying nanoparticle properties," *Nanoscale*, vol. 10, no. 27, pp. 12871–12934, 2018.
- [35] T. Sugimoto and F. Shiba, "Spontaneous nucleation of monodisperse silver halide particles from homogeneous gelatin solution II: silver bromide," *Colloids and Surfaces A: Physicochemical and Engineering Aspects*, vol. 164, no. 2-3, pp. 205–215, 2000.
- [36] G. Hua, L. Zhang, G. Fei, and M. Fang, "Enhanced catalytic activity induced by defects in mesoporous ceria nanotubes," *Journal of Materials Chemistry*, vol. 22, no. 14, pp. 6851–6855, 2012.
- [37] J. Canivet, M. Vandichel, and D. Farrusseng, "Origin of highly active metal-organic framework catalysts: defects? Defects!" *Dalton Transactions*, vol. 45, no. 10, pp. 4090–4099, 2016.
- [38] Y. Xia, Y. Xiong, B. Lim, and S. E. Skrabalak, "Shape-controlled synthesis of metal nanocrystals: simple chemistry meets complex physics?" *Angewandte Chemie International Edition*, vol. 48, no. 1, pp. 60–103, 2009.
- [39] V. V. Kumar and S. P. Anthony, "Antimicrobial studies of metal and metal oxide nanoparticles," in *Surface Chemistry of Nanobiomaterials*, pp. 265–300, Elsevier, Amsterdam, Netherlands, 2016.
- [40] M. Hans, A. Erbe, S. Mathews, Y. Chen, M. Solioz, and F. Mücklich, "Role of copper oxides in contact killing of bacteria," *Langmuir*, vol. 29, no. 52, pp. 16160–16166, 2013.
- [41] L. K. Limbach, P. Wick, P. Manser, R. N. Grass, A. Bruinink, and W. J. Stark, "Exposure of engineered nanoparticles to human lung epithelial cells: influence of chemical composition and catalytic activity on oxidative stress," *Environmental Science & Technology*, vol. 41, no. 11, pp. 4158–4163, 2007.
- [42] S. AlYahya, B. J. Rani, G. Ravi et al., "Size dependent magnetic and antibacterial properties of solvothermally synthesized cuprous oxide (Cu_2O) nanocubes," *Journal of Materials Science: Materials in Electronics*, vol. 29, no. 20, pp. 17622–17629, 2018.
- [43] T. D. Majumdar, M. Singh, M. Thapa, M. Dutta, A. Mukherjee, and C. K. Ghosh, "Size-dependent antibacterial activity of copper nanoparticles against *Xanthomonas oryzae* pv. *oryzae*—a synthetic and mechanistic approach," *Colloid and Interface Science Communications*, vol. 32, p. 100190, 2019.
- [44] B. She, X. Wan, J. Tang, Y. Deng, X. Zhou, and C. Xiao, "Size- and morphology-dependent antibacterial properties of cuprous oxide nanoparticle and their synergistic antibacterial effect," *Science of Advanced Materials*, vol. 8, no. 5, pp. 1074–1078, 2016.
- [45] M. D. Susman, R. Popovitz-Biro, A. Vaskevich, and I. Rubinstein, "pH-Dependent galvanic replacement of supported and colloidal Cu_2O nanocrystals with gold and palladium," *Small*, vol. 11, no. 32, pp. 3942–3953, 2015.
- [46] J. Li and L. McLandsborough, "The effects of the surface charge and hydrophobicity of *Escherichia coli* on its adhesion to beef muscle," *International Journal of Food Microbiology*, vol. 53, no. 2-3, pp. 185–193, 1999.